



HAL
open science

Cd content dependent magnetic properties of $\text{Li}_{0.5-x}/2$ $\text{Cdx Fe}_{2.5-x}/2\text{O}_4$ nano-ferrite prepared without post preparation thermal treatment

Rulan Verma, Shashank Kane, Priyanka Tiwari, S S Modak, Frédéric
Mazaleyrat

► To cite this version:

Rulan Verma, Shashank Kane, Priyanka Tiwari, S S Modak, Frédéric Mazaleyrat. Cd content dependent magnetic properties of $\text{Li}_{0.5-x}/2$ $\text{Cdx Fe}_{2.5-x}/2\text{O}_4$ nano-ferrite prepared without post preparation thermal treatment. *Advances in basic Science (ICABS 2019)*, Feb 2019, Bahal, India. pp.160015, 10.1063/1.5122596 . hal-04453274

HAL Id: hal-04453274

<https://hal.science/hal-04453274>

Submitted on 12 Feb 2024

HAL is a multi-disciplinary open access archive for the deposit and dissemination of scientific research documents, whether they are published or not. The documents may come from teaching and research institutions in France or abroad, or from public or private research centers.

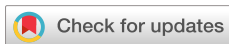
L'archive ouverte pluridisciplinaire **HAL**, est destinée au dépôt et à la diffusion de documents scientifiques de niveau recherche, publiés ou non, émanant des établissements d'enseignement et de recherche français ou étrangers, des laboratoires publics ou privés.

Copyright

RESEARCH ARTICLE | AUGUST 29 2019

Cd content dependent magnetic properties of $\text{Li}_{0.5-x/2} \text{Cd}_x \text{Fe}_{2.5-x/2} \text{O}_4$ nano-ferrite prepared without post preparation thermal treatment

R. Verma; S. N. Kane ; P. Tiwari; S. S. Modak; F. Mazaleyrat



AIP Conf. Proc. 2142, 160015 (2019)

<https://doi.org/10.1063/1.5122596>



CrossMark



Cut Hall measurement time in *half* using an M91 FastHall™ controller



Also available as part of a tabletop system and an option for your PPMS® system

Cd Content Dependent Magnetic Properties of $\text{Li}_{0.5-x/2} \text{Cd}_x \text{Fe}_{2.5-x/2} \text{O}_4$ Nano-Ferrite Prepared Without Post Preparation Thermal Treatment

R. Verma¹, S. N. Kane^{1, a)}, P. Tiwari^{1,2}, S. S. Modak³ and F. Mazaleyrat⁴

¹Magnetic Materials Laboratory, School of Physics, D. A. University, Khandwa road, Indore – 452001, India.

²Department of Physics, Prestige Institute of Engineering Management and Research, Indore - 452010, India.

³Physics Department, Jaypee University of Engineering and Technology, Raghuarh, Guna 473226, India.

⁴SATIE, ENS Universite Paris-Saclay, CNRS 8029, 61 Av. du Pdt. Wilson, F-94230, Cachan, France.

^{a)}Corresponding author: kane_sn@yahoo.com

Abstract. Nano-crystalline $\text{Li}_{0.5-x/2} \text{Cd}_x \text{Fe}_{2.5-0.5/2} \text{O}_4$, ($x = 0.0, 0.11, 0.22, 0.33, 0.44$), were synthesized by sol gel auto combustion method without post preparation thermal treatment. Effect of Cd content on structural, magnetic properties has been studied by x-ray diffraction (XRD), magnetic measurements. XRD validates the formation of spinel ferrite, with Scherrer's grain diameter ranging between 16.7 nm - 28.95 nm. Coercivity (H_c) and anisotropy constant (K_1) values respectively ranges between 115.13 to 178.71 Oe and 1.86×10^4 to 3.68×10^4 erg/cc. Best magnetization of $56.77 \text{ Am}^2/\text{kg}$ was obtained for $x = 0.44$, observed variation of magnetic properties is explained in terms of observed changes in cation distribution.

INTRODUCTION

Ferrites find applications in various fields including those in permanent magnets, high density storage devices, and targeted drug delivery etc. [1]. Spinel ferrites are represented by formula $\text{A}^{2+} \text{B}^{3+}_2 \text{O}_4$, [A^{2+} ; B^{3+} - di-trivalent ions], where A (tetrahedral), B (octahedral) sub-lattices form cubic structure, with oxygen anions occupying face centered cubic (fcc) positions. Spinel ferrites have Fd_3m space group reveal fcc (face centered cubic) structure, with total 56 ion per unit cell, 32 divalent oxygen ions forms closed pack fcc structure with 64 tetrahedral interstitial sites (*A-sites*) and 32 octahedral interstitial sites (*B-sites*), out of available sites only 8 tetrahedral (*A-sites*) and 16 octahedral (*B-sites*) are occupied by divalent and trivalent metal ions. Structural, magnetic properties of ferrites can be modified via suitable substitution of divalent cations [1, 2]. Variation of structure, magnetic properties can also be achieved via: partial or complete substitution; a particular synthesis method; thermal treatment etc. It is remarkable to note that a substitution of a magnetic or a non-magnetic cation modifies the cationic distribution on A, B site, and thus would affect the magnetic interactions, which in-turn will influence the magnetic properties [3].

Literature shows that mixed CdFe_2O_4 ferrite shows normal spinel structure with Cd^{2+} ions have a preference for tetrahedral (A-site). Cd-based ferrites are technologically important due to their resistivity, high permeability, low magnetic losses. Li-ferrite display inverse spinel structure with preference of Li-ions to occupy B-site, and Fe^{3+} ions are distributed on both A, B-site [4]. Lithium ferrite is an exclusive member of the spinel group of ferrimagnetic oxides, and has applications in the field of microwave devices because of its square hysteresis loop, high curie temperature, low microwave dielectric losses, and high saturation magnetization. Li ferrites are used in many electronic devices such as inductors, converters or electromagnetic wave absorbers, phase-shifters, radar, etc. in the radio frequency range, owing to high Curie temperature, high saturation magnetization, and square hysteresis loop. Literature reports, Li-Cd [5], Li-Mg [6], Li-Ni [7], Li-Zn [8], effect of a specific substitution and, a particular synthesis process (e. g. - sol gel auto combustion method, co-precipitation, solid state reaction etc.) on their structural, magnetic properties.

It is worth noting that, sol-gel auto combustion is one of the most efficient methods, for synthesizing nano-materials at relatively lower temperature (~110° C), to obtain desired properties . In sol gel auto combustion method, final phase is even formed in ‘dry gel’ form and, no further sintering would be required so giving a possibility to synthesize ferrites via and energy efficient protocol. Although literature reports Li-Cd based ferrites, though their synthesis via sol-gel auto-combustion method is less-explored in the literature. Hence, in the present work we report the study of structural, magnetic properties of cadmium doped lithium ferrite using sol-gel auto-combustion method, via x-ray diffraction (XRD), magnetic measurements (VSM).

EXPERIMENTAL DETAILS

Here sol-gel auto-combustion method was used to synthesize $\text{Li}_{0.5-x/2}\text{Cd}_x\text{Fe}_{2.5-x/2}\text{O}_4$ spinel ferrites as described in [9]. Samples were prepared by using AR grade nitrate/citrate precursors: [Lithium acetate – $(\text{CH}_3\text{COO})_2\text{Li} \cdot 4\text{H}_2\text{O}$], Cadmium acetate – $(\text{CH}_3\text{COO})_2\text{Cd} \cdot 2\text{H}_2\text{O}$, Ferric nitrate – $(\text{Fe}(\text{NO}_3)_3 \cdot 9\text{H}_2\text{O})$] by mixing them in stoichiometric ratio. Precursors were dissolved in 10 ml de-ionized water keeping metal salt to citric acid ratio as 1:1, maintaining pH of the solution at 7 by adding ammonia solution (NH_4OH). Resulting solution was heated at ~ 110 °C to obtain fluffy powder, called ‘dry-gel’ which was to study their structural, magnetic properties without any post – preparation thermal treatment. XRD measurements (θ -2 θ configuration) were done by Bruker D8 Advance X-ray diffractometer, utilizing fast counting detector (Bruker Linux- eye detector), utilizing $\text{CuK}\alpha$ radiation ($\lambda = 0.154$ nm). Hysteresis loops were measured by Lakeshore Model 7410 (VSM) by applying maximum field - $H_{\text{max}} \approx \pm 1.9$ T. Measured hysteresis loops were used to get coercivity (H_c), saturation magnetization ($M_{s(\text{exp})}$).

DATA ANALYSIS

The lattice parameter (a_{exp}) corresponding to plane [311] was obtained by expression: $a_{\text{exp}} = d\sqrt{h^2 + k^2 + l^2}$, where d – inter-planer spacing and, (h, k, l) - miller indices. a_{exp} was used to obtain the x-ray density (ρ_{XRD}) of the studied samples. Particle size ($D_{\text{W-H}}$) was obtained by Williamson-Hall (W-H) plot, by incorporating both instrumental, and strain broadening [10]. Specific surface area (S) was calculated using the expression: $S = [6 / (D_{\text{W-H}} \times \rho_{\text{XRD}})]$, where $D_{\text{W-H}}$ - particle size and ρ_{XRD} - x-ray density. Cation distribution of the studied samples was obtained by XRD peak intensities employing Bertaut method [11]. Cation distribution of samples was obtained by XRD line intensities using following formula, $\frac{I_{hkl}^{\text{obs}}}{I_{h'k'l'}^{\text{obs}}} = \frac{I_{hkl}^{\text{cal}}}{I_{h'k'l'}^{\text{cal}}}$, where I_{hkl}^{obs} and I_{hkl}^{cal} are observed, and calculated intensities for the reflection (hkl) [11,12]. Best information regarding cation distribution can be obtained by comparing experimental and calculated intensity ratios for reflection. This method selects a pairs of reflections calculated intensities for reflection (hkl). In the present study, (220) (422) (400) (440) planes are considered for cation distribution as these planes are sensitive to distribution of cations among tetrahedral A , octahedral B sites of the spinel lattice. The best cation distribution for tetrahedral and octahedral sites for which, theoretical and experimental intensities ratios agree noticeably are taken to be the accurate one. The calculated, observed intensity ratios were compared for several combinations of cation distribution at A and B-sites. Obtained cation distribution was used to calculate, Néel magnetic moment (theoretical magnetization at 0 K ‘ $M_{s(0)}$ ’, is calculated using formula: $n_N = M_B - M_A$ in Bohr magneton μ_B ,) where M_A is magnetic moment of A-site, M_B is magnetic moment of B-site), oxygen position parameter (u), bond angles ($\theta_1, \theta_2, \theta_3, \theta_4, \theta_5$), and delta parameter (δ). Coercivity (H_c), saturation magnetization (M_s) and, anisotropy constant (K_1), static magnetic losses, canting angle ‘ α_{Y-K} ’ were obtained from hysteresis measurements, X-ray density (ρ_{XRD}) of the studied samples was also calculated by using formula: $\rho_{\text{XRD}} = 8M/N_A a_{\text{exp}}$, where, M = Molecular weight N_A – Avogadro’s number (6.022×10^{23} particles/mol). Particle size D_s , was calculated by Scherrers formula ($D = 0.9 \lambda/\beta \text{Cos}\theta$). Following equation was used to calculate the dislocation density: Dislocation Density = $15 \varepsilon / a_{\text{exp}} D_{\text{W-H}}$, where $D_{\text{W-H}}$ - particle size ($D_{\text{W-H}}$), a_{exp} – Lattice parameter, ε – lattice strain, where $D_{\text{W-H}}$ - particle size and ρ_{XRD} - x-ray density, where λ - Wavelength of x-ray used, β - Line width, θ - Peak position (in 2θ scale). Theoretical lattice parameter (a_{th}) was estimated by using following expression: $a_{\text{th}} = \frac{8}{3\sqrt{3}}[(r_A + R_o) + \sqrt{3}(r_B + R_o)]$, Where, r_A – ionic radius of A-site, r_B – ionic radius of B-site, $R_o = 0.138$ nm (ionic radius of oxygen ion). Oxygen positional parameter (u) was obtained by using following equation $u^{\text{th}} = \frac{(r_A + R_o)}{(\sqrt{3} * a_{\text{exp}})} + \frac{1}{4}$.

RESULTS AND DISCUSSIONS

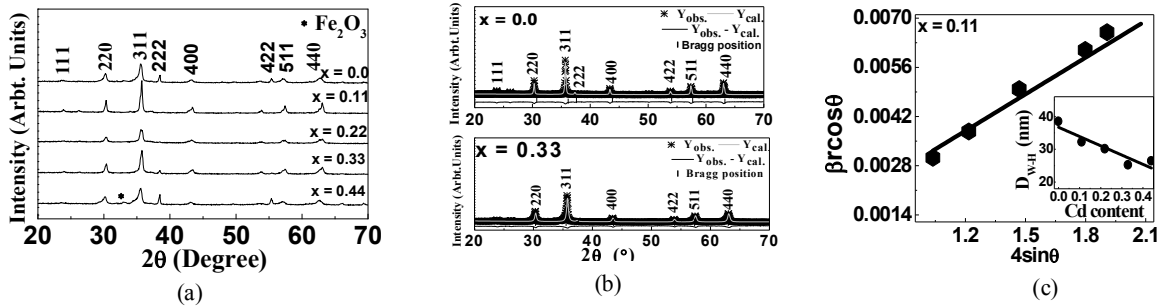


FIGURE 1. (a) XRD pattern (b) Rietveld refinement for $x = 0.11, 0.33$ (c) Williamson-Hall plot for $x = 0.11$, Inset: D_{W-H} with Cd content

XRD patterns of the studied samples, confirm the formation of single phase nano-crystalline cubic spinel structure, shown in figure 1 a, where a small fraction of Fe_2O_3 was also detected for sample with $x = 0.44$. Rietveld refined plot for the sample with $x = 0.00$ and 0.33 , shown in figure 1 b [13]. Representative W-H plot for the sample with $x = 0.11$ is depicted in figure 1 c, was used to obtain particle size (shown as inset), Strain (ϵ), Grain diameter obtained by Scherer's formula (D_s), Williamson-Hall plot (D_{W-H}), specific surface area (S), strain (ϵ), and dislocation density, obtained by analyzing XRD data are illustrated in Table 1. Perusal of table 1 shows that decrease of unit cell volume, overtakes decrease in mass of the unit cell, and is responsible for the increase in ρ_{XRD} [14]. Specific surface area of the studied nano particles increases and range between $41.03\text{--}32.66\text{ m}^2/\text{g}$, S increases. Such non-monotonic variation of S is ascribable to the variation of the particle size of Li-Cd ferrite. In general it is found that strain decreases as Cd^{2+} concentration increases, and expected effect on magnetic properties. Cd^{2+} addition in the samples alters the induced strain (ϵ) in the crystallites (range between $0.0013\text{--}0.0061$).

Figure 1 (c), represents W-H plot (straight line between $4\sin\theta$ (x-axis) and $\beta \cos\theta$ (y-axis)). The slope of the line gives strain (ϵ) and the intercept ($0.9\lambda/D_{W-H}$) with y-axis gives the crystallite size (D_{W-H}) [15]. Particle size (D_s) and (D_{W-H}) respectively range between $16.71\text{--}28.95\text{ nm}$ and $26.45\text{--}38.48\text{ nm}$. Difference between obtained (D_s) and (D_{W-H}) values is ascribable to the fact that for obtaining D_{W-H} , calculated by Williamson-Hall 'W-H' plot (representative W-H plot is shown in figure 2), by incorporating both instrumental, and strain broadening, whereas for calculating D_s instrumental, and strain broadening was not used. Observed changes (shown in table 1) in grain size, crystal strain, and dislocation density are ascribable to crystal deformation leading to changes in magnetic properties [16].

Table 1: Variation of lattice parameter (a_{exp}), Scherrer's grain diameter (D) and (D_{W-H}), cell volume (V), specific surface area (S), x-ray density (ρ_{xrd}), lattice strain (ϵ), dislocation density with Cd content (x).

x	a_{exp} nm	D_s (nm)	D_{W-H} (nm)	S (m^2/gm)	ρ_{xrd} (kg/m^3)	ϵ	Dislocation Density (Lines/m^2)
0.0	0.8321	28.9	38.48	32.66	4773.95	0.0061	2.85×10^{15}
0.11	0.8346	16.0	32.20	37.76	4934.72	0.0023	1.28×10^{15}
0.22	0.8335	19.8	30.12	38.61	5158.32	0.0032	1.91×10^{15}
0.33	0.8357	17.1	25.23	44.69	5320.79	0.0002	0.14×10^{15}
0.44	0.8354	16.7	26.45	41.03	5528.97	0.0013	0.88×10^{15}

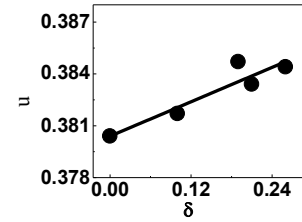


FIGURE 2. Variation of u with δ , line connecting points: linear fit to experimental data

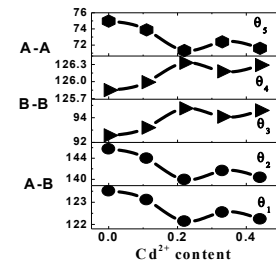


FIGURE 3. Cd dependence of bond angles ($\theta_1, \theta_2, \theta_3, \theta_4, \theta_5$)

Table 2. Cation distribution (for A, B site), inversion parameter (δ), oxygen position parameter (u) of $\text{Li}_{0.5-x/2}\text{Cd}_x\text{Fe}_{2.5-x/2}$ as a function of Cd^{2+} content.

Cation distributions	δ	a_{th} (nm)	u
$(\text{Li}^{1+}_{0.1}\text{Fe}^{3+}_{0.9})^{\text{A}}[\text{Li}^{1+}_{0.4}\text{Fe}^{3+}_{1.6}]^{\text{B}}$	0.90	0.8355	0.380
$(\text{Li}^{1+}_{0.05}\text{Cd}^{2+}_{0.10}\text{Fe}^{3+}_{0.85})^{\text{A}}[\text{Li}^{1+}_{0.395}\text{Cd}^{2+}_{0.01}\text{Fe}^{3+}_{1.595}]^{\text{B}}$	0.85	0.8396	0.381
$(\text{Li}^{1+}_{0.09}\text{Cd}^{2+}_{0.19}\text{Fe}^{3+}_{0.72})^{\text{A}}[\text{Li}^{1+}_{0.30}\text{Cd}^{2+}_{0.03}\text{Fe}^{3+}_{1.67}]^{\text{B}}$	0.72	0.8404	0.384
$(\text{Li}^{1+}_{0.01}\text{Cd}^{2+}_{0.21}\text{Fe}^{3+}_{0.78})^{\text{A}}[\text{Li}^{1+}_{0.325}\text{Cd}^{2+}_{0.12}\text{Fe}^{3+}_{1.555}]^{\text{B}}$	0.78	0.8468	0.383
$(\text{Li}^{1+}_{0.00}\text{Cd}^{2+}_{0.26}\text{Fe}^{3+}_{0.74})^{\text{A}}[\text{Li}^{1+}_{0.28}\text{Cd}^{2+}_{0.18}\text{Fe}_{1.54}]^{\text{B}}$	0.74	0.8414	0.384

Perusal of table 2, shows variation of cation distribution oxygen positional parameter (u), delta parameter (δ) with Cd^{2+} content. Oxygen position parameter (u) increases with increasing Cd^{2+} content, and is due to the migration of Cd^{2+} ions to A-site resulting in its expansion. Observed value of oxygen parameter (u) increases from 0.380 to 0.384, which is slightly greater than its ideal value ($u_{\text{ideal}} = 0.375$) and it could be used as quantitative measurement of oxygen displacement [17]. It is worth noting that variation of u with delta (δ) (is shown in figure 2) attributed to increased distortion in the structure, anticipated to influence the magnetization. Perusal of figure 2 also depicts that in increase degree of inversion also leads to increased distortion, mirrors in changes in M_s , displays the importance of cationic distribution (on A, B site) in shaping magnetic properties.

Figure 3, shows Cd content dependence of bond angles ($\theta_1, \theta_2, \theta_3, \theta_4, \theta_5$). It is worth noting that, strength of the magnetic interactions (A-O-B, B-O-B and A-O-A) are directly proportional to the bond angles. Cd-content dependence of bond angles ($\theta_1, \theta_2, \theta_3, \theta_4, \theta_5$) provides information on A-O-B (θ_1, θ_2), A-O-A (θ_3, θ_4), B-O-B (θ_5) exchange interaction, as shown in fig.3. The bond angles θ_1, θ_2 and θ_5 decreases θ_3, θ_4 increases clearly shows the weakening of A-B and A-A interaction, and strengthening of the B-B interaction is responsible for changes in the magnetic moment reflected in changes in magnetic properties [16, 17].

Table 3. Coercivity (H_c), experimental saturation magnetization (M_s), magnetization at 0K ($M_{s(0K)}$), static magnetic losses, magneto-crystalline anisotropy (K_1) and Yaffet- Kittel angle (α_{y-k}) (obtained from cation distribution) for Li-Cd ferrite.

X	H_c (Oe)	M_s (Am ² /kg)	$M_{s(0k)}$ (Am ² /kg)	Losses J/kg	K_1 erg/cc	α_{y-k} (°)
0.00	178.7	35.9	94.39	1.8598	3.1327×10^4	43.94
0.11	195.8	18.8	96.18	1.1370	1.8625×10^4	51.68
0.22	154.4	39.2	110.50	1.7756	3.1916×10^4	37.82
0.33	158.4	27.7	92.43	1.1547	2.3915×10^4	49.45
0.44	115.1	56.7	92.03	1.8191	3.6889×10^4	37.81

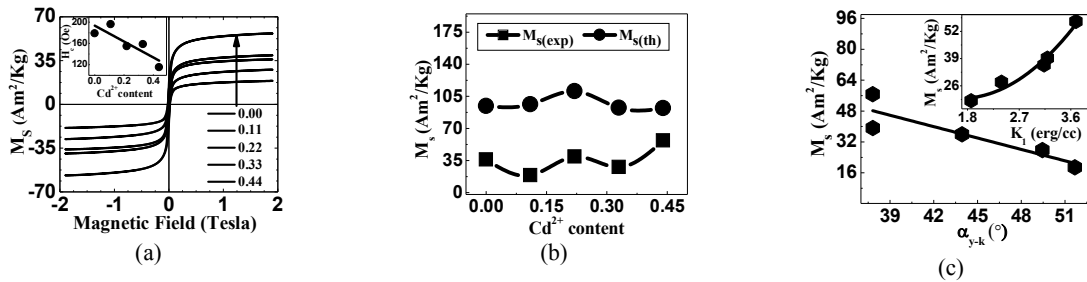


FIGURE 4: (a) Hysteresis loops of Li-Cd ferrite, Inset: Linear variation of H_c , (b) Variation of experimental $M_s(\text{exp})$, $M_s(\text{th})$, (c) Variation of experimental $M_s(\text{exp})$ with α_{y-k} angle, Inset: Variation of $M_s(\text{exp})$ with K_1 .

Table 3, gives coercivity (H_c), experimental saturation magnetization (M_s), magnetization at 0K ($M_{s(0K)}$), magnetic losses (static), magneto-crystalline anisotropy (K_1), and α_{y-k} angle for the studied samples. Observed changes in parameters are due to changes in Cd^{2+} content. Figure 4 (a) depicts hysteresis loops of the studied samples, whereas inset shows linear dependence of H_c with increasing content of Cd. Increase of Cd^{2+} content leads to better soft magnetic behavior (lowering of H_c and increase of M_s) Figure 4 (b) shows similar trend of

experimental $M_{s(\text{exp})}$ at 300 K (obtained from VSM measurements) and that of theoretical magnetization at 0 K: $M_{s(0)}$, shows that the magnetic behavior of the studied annealed samples depicts the cation distribution (used to get M_s) is close to [18]. Both M_s and K_1 exhibit similar trend, is in accordance with expression.

Figure 4 c, shows linear variation of M_s with nonzero value of Yaffét- Kittel angle (α_{y-k}), inset graph shows variation of magneto crystalline-anisotropy (K_1) with M_s , reduction of M_s with increase of α_{y-k} is attributed to spin canting at surface [19].

SUMMARY

To summarize sol-gel auto-combustion method was used to synthesize Cd^{2+} doped Li-ferrite, inversion parameter where no thermal treatment was applied. XRD reveals the formation of spinel structure. Grain diameter (D_{W-H}) varies between 17.27 – 42.28 nm. Experimental lattice parameter (a_{exp}), X-ray density (ρ_{XRD}) increase with the increasing content of Cd^{2+} ascribed to ionic difference of Li^{1+} , Cd^{2+} , Fe^{3+} . Results reveal that the cation distribution on A, B sites is in close agreement with real distribution on A and B-sites. The structural parameters: ionic radii on A-site (r_A) and B-site (r_B), oxygen position parameters, show considerable changes with increasing Cd^{2+} content. Observed changes in magnetic properties is explained in terms of changes in Cd^{2+} ion content dependent A-B, B-B, A-B interactions, cationic distortion and spin canting at the surface of the nano particles.

ACKNOWLEDGMENTS

Authors thank Dr. M Gupta, UGC-DAE CSR, Indore for XRD measurements. S. N. Kane acknowledges gratefully one month hospitality as invited professor at Ecole Normale Supérieure de Cachan, University Paris-Saclay (France), during Nov.-Dec. 2017.

REFERENCES

1. S. N. Kane, S. Raguwanshi, M. Satalkar, V. R. Reddy, U. P. Deshpande, T. R. Tatarchuk and F. Mazaleyrat, *AIP Conf. Proc.* **1953**, 030089-4 (2018).
2. T. Tatarchuk, M. Bououdina, W. Macyk, O. Shyichuk, N. Paliychuk, I. Yaremiy, B. Al-Najar and M. Pacia, *Nanoscale Res. Lett.* **12**, 141-11 (2017).
3. J. Smit, H. P. J. Wijn, Ferites, Philips Technical Library, Eindhoven, (1959).
4. S. Raghuvanshi, F. Mazaleyrat, and S. N. Kane, *AIP Advances* **8**, 047804–1–047804-11 (2018).
5. A. M. Shaikh, S. S. Bellad and B. K. Chougule, *J. Magn. Magn. Mater.*, **195**, 384–390 (1999).
6. M. M. Hessian, *Journal of Magnetism and Magnetic Materials*, **320**, 2800–2807 (2008).
7. S. S. Bellad, R. B. Pujar, B. K. Chougule, *Materials Chemistry and Physics*, **52**, 166–169 (1998).
8. S. Panchal, S. Raghuvanshi, K. Gahlot, F. Mazaleyrat and S. N. Kane, *AIP Advances* **6**, 055930–6 (2016).
9. R. G. Kharabe, R. S. Devan, C. M. Kanamadi and B. K. Chougule, *Smart Mater. Strut.* **15**, N36–N39 (2006).
10. D. R. Mane, S. Patil, D. D. Birajdar, A. B. Kadam, S. Shirsath and R. H. Kadam, *Mater. Chem. Phys.*, **126**, 755–760 (2011).
11. E. F. Bertaut, *C. R. Acad. Sci.* **230**, 213 (1950).
12. S. N. Kane and M. Satalkar, *J. Mater. Sci.* **52**, 3467–3477 (2017).
13. L. Gastaldi and A. Lapicciarella, *J. Solid State Chem.* **30**, 223 (1979).
14. L. Lutterotti and P. scardi, *J. Appl. Cryst* **23**, 246-252 (1990).
15. A. Kolhatkar, A. C. Jamison, D. Litvinov and T. R. Lee, *Int. J. Mol. Sci.* **14(8)**, 15977–16009 (2013).
16. R. Verma, S. N. Kane, S. Raghuvanshi, M. Satalkar, S. S. Modak and F. Mazaleyrat, *AIP Conf. Proc.* **1953**, 030135-1-030135-4 (2018).
17. S. K. Emdadul Islam, P. Sharma, *J. Nano- Electron Phys.* **6**, 01008 (2014).
18. S. K. Nath, K. H. Maria, S. Noor, S. S. Sikder, S. M. Hoque, M. A. Hakim, *J. Magn. Magn. Mater.* **324**, 2116–2120 (2012).
19. G. Barrera, M. Coisson, F. Celegato, S. Raghuvanshi, F. Mazaleyrat, S. N. Kane and P. Tiberto, *J. Magn. Magn. Mater.* **456**, 372–380 (2018).